THE JOURNAL OF PHYSICAL CHEMISTRY C

ARTICLE

pubs.acs.org/JPCC

Photoelectrochemical Oxidation of Water Using Nanostructured $BiVO_4$ Films

Sean P. Berglund,[†] David W. Flaherty,[†] Nathan T. Hahn,[†] Allen J. Bard,[‡] and C. Buddie Mullins[†,‡,*]

[†]Department of Chemical Engineering, [‡]Department of Chemistry and Biochemistry, Center for Electrochemistry, Texas Materials Institute, and Center for Nano- and Molecular Science, University of Texas at Austin, 1 University Station C0400, Austin, Texas 78712-0231, United States

Supporting Information

ABSTRACT: Nanostructured $BiVO_4$ films were synthesized by coevaporation of bismuth and vanadium in an oxygen ambient, a process referred to as reactive ballistic deposition (RBD). The films were tested in various electrolyte solutions to assess their activity for photoelectrochemical water oxidation. Deposition parameters, including the V/Bi atomic flux ratio and the incident angle of deposition, were adjusted. Films deposited with excess vanadium (V/Bi = 2) and incident angles of deposition at 65° showed the highest initial photocurrents with IPCE values above 21% for light wavelengths of 340−460 nm (in 0.5 M Na_2SO_4 at 1.0 V vs Ag/AgCl). With continued illumination the excess vanadium in these films dissolved into the electrolyte and the photocurrents dropped by 60−75% before reaching steady state. The steady-state photocurrent and IPCE values (above 14% for 340−460 nm light) were higher than the initial values for films synthesized with stoichiometric amounts of vanadium and bismuth (V/Bi = 1) and incident angles of deposition at 65°. Stoichiometric $BiVO_4$ films remained stable under illumination but their photocurrents were limited by surface reaction kinetics. The addition of cobalt as an electrocatalyst to the surface of these films increased their photocurrent by a factor of 3.

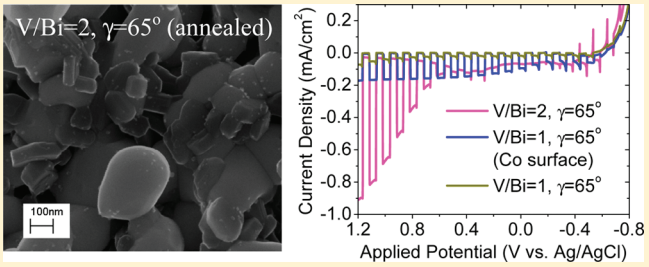

INTRODUCTION

Photoelectrochemical splitting of water into hydrogen and oxygen has great potential for solar energy conversion and storage. Since the first experimental demonstration of photoelectrochemical water splitting using TiO_2 in the 1970s,[1] many different semiconductor materials have been tested.[2−5] However, none of these have been put into practical use in a large scale system. In order to efficiently split water, a photoelectrochemical system must meet many requirements. The system must be composed of materials with band gaps small enough (<3.0 eV) to absorb a large portion of the solar spectrum including visible light. Concurrently, the conduction and valence bands of the materials must straddle the proton reduction and water oxidation redox potentials. The materials should promote facile charge transfer and have high surface area with active sites for both proton reduction and water oxidation. Lastly, the system should be composed of materials that are inexpensive and long lasting; otherwise, it will not be practical for large scale energy conversion.[6] To date, no known materials satisfy all the above requirements for efficient and cost-effective water splitting.

Recently, $BiVO_4$ has attracted attention due to its high photocatalytic activity for oxygen evolution in aqueous solutions under visible light irradiation relative to other known materials tested under similar conditions.[2] $BiVO_4$ exists in three main polymorphs: the zircon structure with a tetragonal crystal system and the scheelite structure with monoclinic and tetragonal crystal systems. The monoclinic crystal system has been reported as the most photoactive form of $BiVO_4$.[7,8] The bandgap of monoclinic $BiVO_4$ has been shown to be 2.3−2.4 eV by experiment[7,9−11] and 2.16 eV (direct band gap) from density functional theory (DFT) calculations.[12] Based on the stoichiometry of $BiVO_4$, the oxidation states and atomic orbitals are given by Bi^{3+} ($5d^{10}6s^2$), V^{5+} ($3d^0$), and O^{2-} ($2p^6$). The valence band is formed by coupling of Bi 6s and O 2p orbitals while the conduction band is primarily controlled by V 3d orbitals, with contributions from the O 2p and Bi 6p orbitals.[12,13] The conduction band edge of $BiVO_4$ has been estimated to be at 0 V vs NHE at pH 0,[14] which corresponds to a valence band edge of 2.4 V vs NHE at pH 0 (using 2.4 eV as the band gap). Because the conduction band is not more negative than the H^+ reduction potential (0.0 V vs NHE at pH 0), pure $BiVO_4$ cannot evolve substantial amounts of H_2 from H_2O without an applied bias on an inert metal counter-electrode. Even with the addition of Pt as an electrocatalyst, $BiVO_4$ did not show activity for H^+ reduction when illuminated in an aqueous methanol (hole-scavenging) solution.[15] On the other hand, the valence band of $BiVO_4$ is below the water

Received: November 16, 2010
Revised: January 14, 2011
Published: February 16, 2011

oxidation potential (1.23 V vs NHE at pH 0), indicating that $BiVO_4$ is thermodynamically capable of evolving O_2 from H_2O. Several researchers have confirmed that $BiVO_4$ can oxidize water by measuring O_2 evolution from aqueous solutions containing Ag^+ as a sacrificial reagent (Ag^+/Ag redox potential at 0.7991 V vs NHE[16]).[7,8,15,17,18] Although $BiVO_4$ is not able to reduce H^+, it is still a promising material for water splitting as the photoanode in a multiphoton photoelectrochemical cell (PEC).

A variety of synthesis techniques have been used to produce $BiVO_4$ for photocatalytic testing. $BiVO_4$ was first synthesized for photocatalytic testing by solid-state reaction of Bi_2O_3 and NH_4VO_3 at high temperatures (970−1170 K)[15] and later by an aqueous process at room temperature using layered compounds of KV_3O_8 and $K_3V_5O_{14}$ with $Bi(NO_3)_3$, which showed improved photocatalytic activity.[7] Since then $BiVO_4$ has been prepared by room temperature hydrolysis,[8] metal−organic decomposition,[19,20] chemical bath deposition,[21] various hydrothermal routes,[17,22,23] the sol−gel method,[10] solution combustion,[24] flame and ultrasonic spray pyrolysis,[25,26] coprecipitation,[27,28] electrosynthesis,[29] and flame-assisted synthesis.[30] Numerous researchers have modified the aqueous and hydrothermal routes with additional precursors,[31] morphology directing reagents,[32−34] sonication,[35] reflux,[36,37] and microwave irradiation.[38] With the exception of solid-state synthesis, the above methods involve some form of wet chemical processing. The present paper discusses the photocatalytic activity of $BiVO_4$ prepared by a vacuum deposition process in which pure bismuth and vanadium were coevaporated in the presence of oxygen as a reactant gas. This deposition process is often referred to as reactive ballistic deposition (RBD) and is described in more detail later.[39−45] RBD can have advantages over wet chemistry methods including simultaneous control of the chemical composition and morphology during synthesis, and the elimination of additional reagents that may be required for wet chemical processing that are not desired in the final material.

In order to accurately assess the activity of a material for photoelectrochemical water splitting it is important to check several key metrics including solar to hydrogen (STH) efficiency, incident photon-to-current efficiency (IPCE), and absorbed photon-to-current efficiency (APCE).[46] Experimentally, $BiVO_4$ has not been proven to evolve H_2 so the STH efficiency cannot be determined without applying a bias between the working and counter-electrode. Efficiencies for O_2 evolution can be calculated, but only a fraction of the recent studies on $BiVO_4$ report such information. A variety of solution species have been used in the study of the photocatalytic properties of $BiVO_4$ including $AgNO_3$, $Fe(NO_3)_3$, Na_2SO_4, NaOH, rhodamine B, methylene blue, and methyl orange. Of these solutions, Na_2SO_4 is the most relevant to direct water splitting because the ionic species (Na^+ and SO_4^{2-}) will not react electrochemically at potentials between −0.414 and 0.816 V vs NHE (thermodynamic redox potentials for water splitting at pH 7). Some researchers have reported IPCE values for $BiVO_4$ using three-electrode photoelectrochemical cells containing Na_2SO_4 as the electrolyte. Particulate films of $BiVO_4$ synthesized by the sol−gel method showed IPCE values at ca. 0.01% (at 1.0 V vs Ag/AgCl) for 380−460 nm light,[10] and $BiVO_4$ synthesized by ultrasonic spray-pyrolysis showed IPCE values up to ca. 2% (at 0.7 V vs SCE) for 450 nm light[47] in 0.1 M Na_2SO_4. In 0.5 M Na_2SO_4 with an applied bias of 1.0 V vs Ag/AgCl under 380−460 nm light, particulate $BiVO_4$ prepared by laser ablation had IPCE values of ca. 0.5−2.5%,[48] whereas $BiVO_4$ synthesized by room temperature hydrolysis had IPCE values of 1−2%,[49] and $BiVO_4$ films prepared by modified metal−organic decomposition were on the order of 1−5%.[50] Modified metal−organic decomposition was also used to produce $BiVO_4$ with the highest IPCE values reported to date in 0.5 M Na_2SO_4 at 1.0 V vs Ag/AgCl, which was ca. 20% for 380−440 nm light.[9] We have used RBD to alter the chemical composition and morphology of $BiVO_4$ films and enhance activity for photoelectrochemical water oxidation. Films synthesized with excess vanadium had initial IPCE values above 21% and steady-state values above 14% in 0.5 M Na_2SO_4 at 1.0 V vs Ag/AgCl for light wavelengths of 340−460 nm, and films synthesized with stoichiometric $BiVO_4$ had IPCE values up to 1.2%.

EXPERIMENTAL SECTION

Photoelectrochemical tests were conducted using a custom three-electrode photoelectrochemical cell. The working electrode was a $BiVO_4$ film with an illumination area of 0.212 cm^2, the counter electrode was a platinum wire, and the reference electrode was a Ag/AgCl reference electrode (CH Instruments, CH111). The cell was controlled using CH Instruments potentiostats (CHI 832 and CH 660D). LSV scans were run from negative to positive potentials with a scan rate of 0.25 V/s. The illumination source was a filtered 100-W xenon lamp (Newport) positioned to provide light intensity close to AM1.5. Visible light was achieved using a colored glass filter (Newport, cut-on 420 nm). IPCE measurements were performed using a mini monochromator (Newport), and the power of each wavelength was measured using a hand-held optical power meter with a UV enhanced Silicon photodetector (Newport). IPCE values were calculated using the following equation:

$$\mathrm{ICPE}(\lambda) = \frac{1240 j_p(\lambda)}{\lambda E_\lambda(\lambda)}$$

where $j_p(\lambda)$ is the measured photocurrent density (mA/cm^2) and $E_\lambda(\lambda)$ is the incident light power density (mW/cm^2) for each wavelength, λ (nm). The electrolyte solutions were made using demineralized water, Na_2SO_4 anhydrous, Na_2SO_3 anhydrous, sodium phosphate monobasic monohydrate, and sodium phosphate dibasic anhydrous (Fisher). Equal parts 1 M phosphate monobasic and 1 M phosphate dibasic were used to make the phosphate buffer solution. The pH of each solution was checked using a benchtop pH meter (OAKTON).

UV−vis transmission spectroscopy measurements were performed using a Cary 5000 spectrophotometer. For Tauc plots the absorption coefficient (α) was determined by:

$$\alpha = \frac{-\ln(10^{-\text{absorbance}})}{z}$$

where z is the film thickness. X-ray diffraction (XRD) measurements were taken on a Bruker-Nonius D8 diffractometer. The Cu Kα radiation source was operated at 40 kV and 40 mA, and measurements were carried out in the $\theta/2\theta$ mode with an incident angle of 5°. Scanning electron microscope (SEM) images were acquired using a LEO 1530 SEM with 10 kV focus voltage and 30 μm aperture. $BiVO_4$ films deposited on substrates were broken in half and viewed on the SEM to obtain film thickness measurements. Film thickness was also verified using a Veeco NT9100 Optical Profiler scanning from bare FTO to the center of the $BiVO_4$ film. X-ray photoelectron spectroscopy (XPS) measurements were performed on a Kratos AXIS Ultra DLD spectrometer with Mg Kα radiation. The concentration of

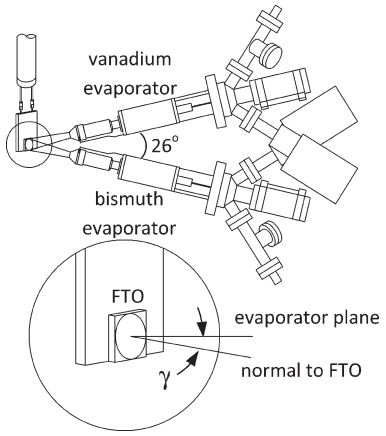

Figure 1. Schematic of sample and evaporator positioning inside the vacuum chamber. The deposition angle (γ) is the angle between the evaporator plane and the normal vector of the FTO substrate surface.

Bi, V, O, and C were calculated from the integrated peak areas obtained after subtracting the background from each peak using the Shirley method.[51] Electrochemical impedance spectroscopy (EIS) measurements were conducted using the CH Instruments CH660D potentiostat, and the built in software was used to create Mott−Schottky plots based on ideal semiconductor behavior.[16] Samples for inductively coupled plasma mass spectrometry (ICP-MS) were diluted 100× and 1000× and measured using an Agilent 7500ce Quadrupole ICP-MS with He as the collision gas to exclude any Cl:O overlap with mass 51 (vanadium).

Description of Synthesis Parameters. The $BiVO_4$ films were synthesized using a high vacuum chamber equipped with two electron beam evaporators (Omicron, EFM 3s), an x-y-z sample manipulator mounted upon a rotary seal, and a quartz crystal microbalance (QCM) and controller (Maxtek Inc.), which have been described previously.[42] For a typical film synthesis, 1.5 cm × 1.5 cm fluorine-doped tin oxide (FTO) coated glass substrates (Pilkington, TEC15) were cleaned and sonicated in ethanol and rinsed with demineralized water before loading into the vacuum chamber. Bismuth granules (Alfa Aesar, 99,997% purity) in a molybdenum crucible were loaded into one evaporator and a 0.25 in. diameter vanadium rod (ESPI, 3N purity) was loaded into the other evaporator. The two evaporators were held in the same vertical plane and aimed at the center of the FTO substrate. This resulted in a 26° difference in direction of the flux from each evaporator. The sample manipulator was positioned approximately 10 cm away from each evaporating component, and the deposition angle (γ) was adjusted to a fixed angle (0−90°) between the direction normal to the surface of the FTO and the evaporator plane as shown in Figure 1 (note that when γ = 0° there is actually an angle of 13° between each evaporator and the direction normal to the FTO surface). After the FTO substrates were loaded, the vacuum chamber was pumped down to a base pressure below 5×10^{-8} Torr. A QCM was used to measure the deposition rate of each component (bismuth and vanadium) separately before starting film growth. The QCM-measured deposition rate and the deposition angle were used to determine the atomic flux of each component and the deposition time required for the target film thickness. After the deposition rate was checked, the chamber was backfilled with oxygen (Matheson, UHP grade) to approximately 6×10^{-6} Torr and films were deposited on the FTO substrates at the ambient temperature of the chamber. The films were removed from the vacuum chamber and annealed to 500 °C in air for 2 h using a muffle

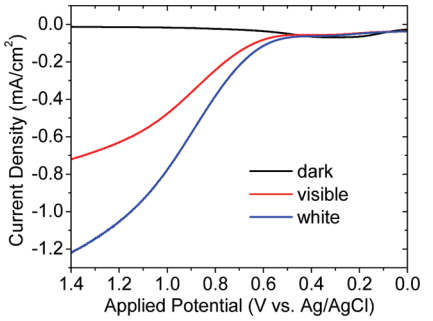

Figure 2. Linear sweep voltammogram of $BiVO_4$ film synthesized by RBD (V/Bi = 2, γ = 65°, thickness = 0.5 μm) in 0.5 M Na_2SO_4 without irradiation (dark) and under illumination with visible light (visible) and white light (white) from a xenon lamp. The scan rate was 0.025 V/s.

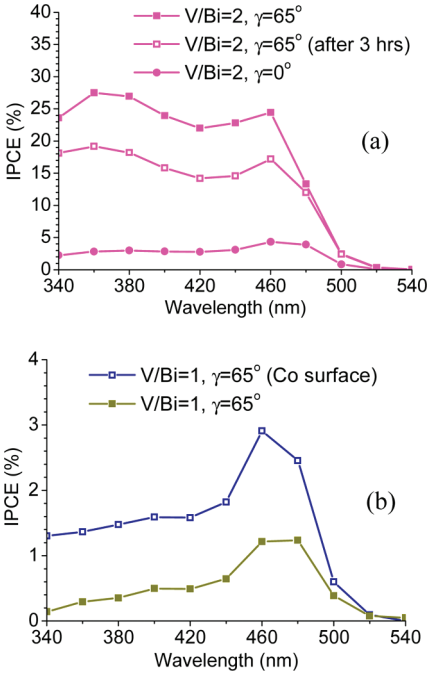

Figure 3. IPCE spectra for films synthesized with different V/Bi atomic ratios, deposition angles (γ), and surface treatments in 0.5 M Na_2SO_4 at an applied potential of 1.0 V vs Ag/AgCl. Both films deposited at V/Bi = 2 (a) had the same initial mass of material, and all films deposited at γ = 65° (a, b) were approximately 0.5 μm thick.

furnace (Neytech) with a temperature ramp rate of 10 °C/min. Lastly, some of the films were submerged in 0.1 M $AgNO_3$ (Acros, 99.85% purity) or 0.1 M $Co(NO_3)_2$ (Alfa Aesar, 99.999% purity) for about 1 h and then rinsed with demineralized water. This was done to add an electrocatalyst to the surface of the films, but we did not measure the oxidation states or relative amounts of Ag or Co that remained on the surface. Other researchers have reported similar surface treatments using $AgNO_3$ and $Co(NO_3)_2$.[9,52]

RESULTS

Photoelectrochemical and Optical Measurements. We attempted to optimize the photocatalytic activity of the $BiVO_4$ films synthesized by varying several important deposition parameters. Films were deposited using a V/Bi atomic flux ratio ranging from 1.0 to 2.9 and a deposition angle (γ) between 0° and 75°. Deposition time was varied to create films with total

dx.doi.org/10.1021/jp1109459 |J. Phys. Chem. C 2011, 115, 3794–3802

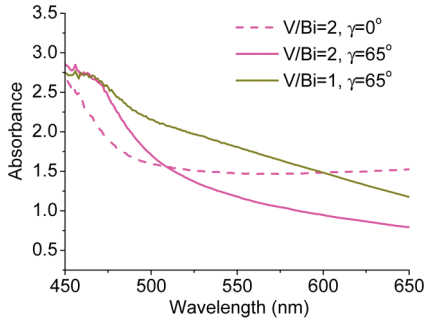

Figure 4. UV−vis absorbance spectrum for films deposited with different V/Bi atomic ratios and deposition angles (γ). Films deposited at V/Bi = 2 had the same mass of material, and both films deposited at γ = 65° were approximately 0.5 μm thick.

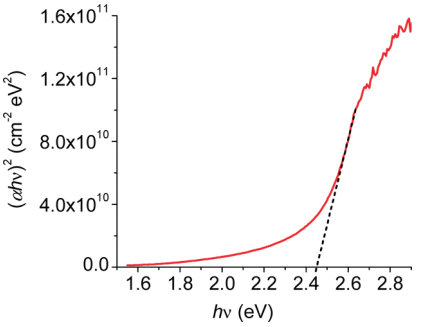

Figure 5. Tauc plot of film synthesized with deposition parameters resulting in highest photoactivity (V/Bi = 2, γ = 65°, thickness = 0.5 μm) pointing to a band gap of approximately 2.45 eV.

thicknesses between approximately 0.2 and 1 μm. The annealing temperature was kept constant at 500 °C because there did not appear to be a significant difference in photocatalytic activity for films annealed in the range of 450−550 °C. Films were tested with and without $AgNO_3$ or $Co(NO_3)_2$ surface treatment. Out of all the films synthesized, those deposited with a V/Bi atomic ratio of approximately two, an angle of incidence between 45° and 75°, and a final film thickness of approximately 0.5 μm consistently showed the highest initial photocurrents under white light illumination in 0.5 M Na_2SO_4 at an applied potential of 1.0 V vs Ag/AgCl. Figure 2 shows a typical linear sweep voltammogram (LSV) for a film synthesized using the above synthesis parameters. The film had an onset potential of about 0.45 V vs Ag/AgCl, and visible light (wavelengths greater than 420 nm) accounted for more than 50% of the total photocurrent when compared to white light (visible light + wavelengths less than 420 nm).

V/Bi atomic ratio and deposition angle (γ) had a significant impact on the photocatalytic activity of the films synthesized by RBD. Figure 3 shows the initial IPCE values obtained for films deposited with different V/Bi atomic ratios, deposition angles, and surface treatments. The two films deposited with V/Bi = 2, γ = 65° and V/Bi = 2, γ = 0° (both shown in Figure 3a) contained the same total mass of material. The film deposited with V/Bi = 2 and γ = 65° (Figure 3a) and the film deposited with V/Bi = 1 and γ = 65° (Figure 3b) were each approximately 0.5 μm thick while the thickness of the film deposited at γ = 0° (Figure 3a) could not be determined because it was composed of nanowires (SEM images shown later). As shown in Figure 3a, the film synthesized using the optimal deposition parameters (V/Bi = 2, γ = 65°) had the highest initial IPCE values. After this

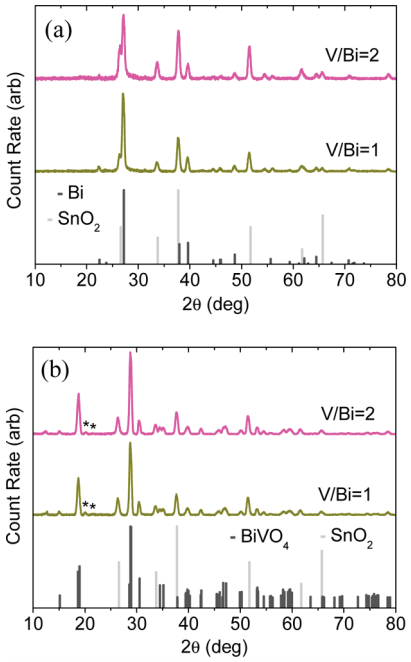

Figure 6. XRD spectrum for $BiVO_4$ films (γ = 65°, thickness = 0.5 μm) with V/Bi = 2 and V/Bi = 1. As deposited (a) and after annealing at 500 °C for 2 h (b). JCPDS peak intensities and locations are plotted below the data for SnO_2 (00-046-1088), crystalline Bi (00-044-1246), and monoclinic $BiVO_4$ (01-075-2480). The * symbol indicates the highest intensity JDCPS peaks for V_2O_5 (01-089-0611).

film was illuminated for 3 h at a constant potential of 1.0 V vs Ag/AgCl, the IPCE values dropped but remained well above the IPCE values for all other films. For wavelengths less than 460 nm, the IPCE values remained at least 4 times higher than films deposited with the same V/Bi ratio at γ = 0° and 14 times higher than films deposited with stoichiometric $BiVO_4$ (V/Bi = 1) at γ = 65°. Films deposited with V/Bi = 1 and γ = 0° had negligible photocurrents and efficiencies so the data is not included. Co was added to the surface of the film with V/Bi = 1 and γ = 65° and improved the photoelectrochemical water oxidation efficiency as shown in Figure 3b. The addition of Co to the surface of the films synthesized with V/Bi = 2 did not improve the efficiency. For all of the films, IPCE values dropped off rapidly for wavelengths higher than 460 nm and approached 0% at 520 nm as expected for a material with a band gap around 2.4 eV (517 nm light).

UV−vis measurements were performed to determine differences in optical properties for the films synthesized with different deposition parameters. Figure 4 shows the UV−vis absorbance spectrum for the three films synthesized with different V/Bi ratios and deposition angles. The spectrum for the film deposited at γ = 0° showed a relatively high and flat UV−vis absorbance for light with wavelengths above 500 nm. The flat section of absorbance was likely caused by diffuse reflection and scattering from the 100−300 nm diameter nanowires observed in these films. For the films deposited with a higher angle of incidence (γ = 65°), only the film deposited with flux of vanadium higher than that of bismuth (V/Bi = 2) showed a sharp absorption onset. The Tauc plot for this film is shown in Figure 5 and points to a direct band gap of 2.45 eV, which is close to the experimentally determined band gap of 2.4 eV for monoclinic $BiVO_4$ synthesized by other methods.[7,9,10]

XRD measurements were performed on the $BiVO_4$ films as deposited (Figure 6a) and after annealing to 500 °C for 2 h

dx.doi.org/10.1021/jp1109459 |J. Phys. Chem. C 2011, 115, 3794–3802

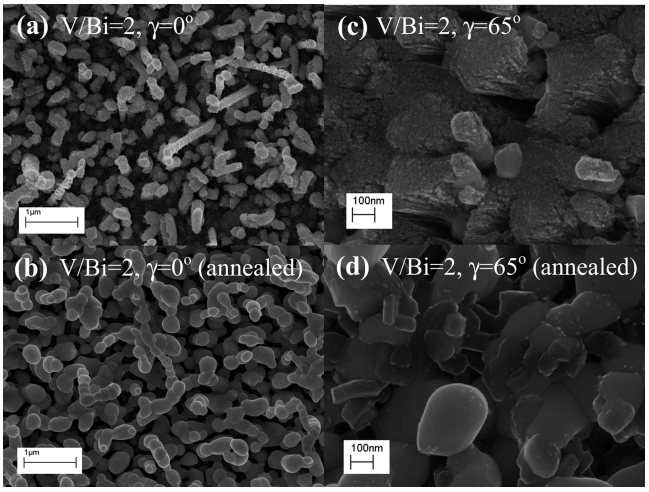

Figure 7. SEM images of films deposited with the same total amount of material and a V/Bi atomic ratio of 2, but different deposition angles of $\gamma = 0°$ (a, b) and $\gamma = 65°$ (c, d) . Images a and c are as-deposited, and images b and d are after annealing at 500 °C for 2 h.

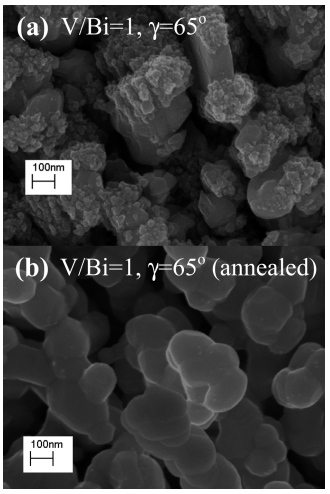

Figure 8. SEM image of a film synthesized by RBD (V/Bi = 1, $\gamma = 65°$, thickness = 0.5 μm). Image a is as-deposited, and image b is after annealing at 500 °C for 2 h.

(Figure 6b). As deposited, all films showed XRD peaks for SnO_2 from the FTO substrate along with crystalline bismuth, JCDPS 00-046-1088 and 00-044-1246, respectively. Films deposited with lower V/Bi ratios (a larger relative mass of bismuth) showed higher intensity peaks for crystalline bismuth relative to the SnO_2 peaks. As deposited, there were no vanadium, bismuth oxide, vanadium oxide, or bismuth vanadate peaks. After annealing, all films showed strong peaks for SnO_2 and monoclinic $BiVO_4$ (JCDPS 01-075-2480). The two tiny peaks at 2θ values of 20.1° and 21.5° match up with two of the highest intensity peaks in the XRD pattern for V_2O_5 (JCPDS 01-089-0611) so there is some segregation of Bi and V even when the two components are deposited in equal amounts. However, the XRD patterns for V/Bi = 1 and V/Bi = 2 after annealing were almost identical, and the highest $BiVO_4$ peak was 26 times more intense than the highest V_2O_5 peak. This suggests that excess vanadium is incorporated into the interstitial sites of films deposited with V/Bi = 2.

The nanostructure and morphology of the films was observed using a SEM. Figures 7 and 8 show SEM images for three different films before and after annealing at 500 °C for 2 h. Films that were deposited at $\gamma = 0°$ consisted of randomly oriented nanowires with diameters on the order of 100−300 nm as shown in Figure 7a. This was seen for all V/Bi atomic ratios that were tested. More glancing angles of incidence ($\gamma = 65°$) produced films with jagged, finely structured surfaces as shown in Figure 7c and Figure 8a. Before annealing, the films deposited at $\gamma = 65°$ show many fine features on the order of 10 nm or smaller. These features appear to sinter and smooth out after annealing to 500 °C, resulting in irregular-shaped features 50−400 nm in size (Figures 7d and 8b). On the basis of these SEM images, annealing appears to reduce the surface area of the films.

The dramatic differences in morphology and surface structure between films deposited at $\gamma = 0°$ and $\gamma = 65°$ can partially be explained by the mechanism of RBD at glancing angles. Several researchers have studied the mechanism for film growth by ballistic deposition (BD) from a single evaporating component at oblique angles of incidence.[53,54] During the initial stages of BD at oblique angles of incidence, incoming atoms randomly land on the substrate surface, creating topographically elevated clusters of atoms. With continued film growth, the elevated clusters promote "self-shadowing", which often causes the film to grow porous, angled columns. The exact morphology and nanostructure of the resulting film is controlled by the self-shadowing effect and surface diffusion of the incoming atoms. Reactive ballistic deposition (RBD) involves the addition of a nondirectional background gas which reacts with the incoming atoms on the surface of the film during deposition.[39] For coevaporation of bismuth and vanadium at $\gamma = 0°$ (13° angle between each evaporator and the direction normal to the substrate), there was essentially no self-shadowing but there was surface diffusion. According to the Movchan and Demchishin structure zone model (SZM),[54−56] surface diffusion during film growth can be related to the ratio of the melting point of the depositing metal (T_m) and the temperature of the substrate (T_s). The melting point of bismuth (271.4 °C) is much lower than that of vanadium (1890 °C). With the FTO left at ambient (near 25 °C) during deposition, bismuth was near the bulk diffusion region ($T_s/T_m > 0.5$) of the Movchan and Demchishin SZM, while vanadium was in the region without significant diffusion ($T_s/T_m < 0.3$). Under these conditions, it is expected that the rate of bismuth adatom diffusion is much greater than that of vanadium. In addition, bismuth adatoms did not appear to react with the background oxygen in the vacuum chamber during deposition. This was determined by measuring the deposition rate of bismuth while gradually leaking in oxygen (the measured deposition rate did not change in the presence of oxygen) and by analyzing the XRD data of films as deposited (peaks are observed for crystalline bismuth metal but not for bismuth oxide). On the other hand, vanadium readily reacts with oxygen during deposition. When vanadium was evaporated while gradually increasing the partial pressure of oxygen, the measured deposition rate increased until it reached a maximum as the material forming on the QCM changed from vanadium metal to vanadium oxide. At low incident angles of deposition ($\gamma \approx 0°$), the observation of nanowires is likely the result of a growth mechanism dominated by surface diffusion and segregation of bismuth atoms. It is also possible that bismuth or vanadium acts as a catalyst for vapor−liquid−solid (VLS) nanowire growth, which involves dissolution

and subsequent precipitation of one of the components when a two-component system is held above the eutectic point.[57] There is limited experimental phase-equilibria data available for the bismuth−vanadium system, especially for the pressures that were used during deposition (6×10^{-6} Torr), but it is plausible that the deposition conditions result in a eutectic point. Available phase diagrams show very low solubility of condensed phase bismuth (~20 ppm) in vanadium near the melting point of bismuth.[58] At higher deposition angles ($\gamma = 45-75°$), the self-shadowing effect becomes more important than surface diffusion, resulting in greater dispersion of bismuth and vanadium atoms so that nanowire growth by dissolution and subsequent precipitation cannot occur. For this reason, films deposited at $\gamma = 65°$ showed a more porous, finely structured surface.

Sacrificial Reagent Photoelectrochemical Measurements. It would not be practical to run a large-scale energy conversion system at an applied potential of 1.0 V vs Ag/AgCl because the energy input required to sustain the bias would negate the energy output.[46] Furthermore, the thermodynamic water oxidation potential in Na_2SO_4 is less than 1.0 V vs Ag/AgCl. The main reason for conducting PEC tests in Na_2SO_4 at 1.0 V vs Ag/AgCl was to compare the activity of $BiVO_4$ films synthesized by RBD with that of $BiVO_4$ synthesized by other techniques.[9,48−50] At such a positive bias, films deposited with excess vanadium (V/Bi = 2) showed higher photocatalytic activity than films deposited with equal amounts of bismuth and vanadium (V/Bi = 1), but this is not always the case for different electrolytes and lower applied biases. For example, particulate $BiVO_4$ prepared using layered compounds of KV_3O_8 and $K_3V_5O_{14}$ with $Bi(NO_3)_3$ showed the highest O_2 evolution rate from 0.05 mol/L $AgNO_3$ when the starting materials had a V:Bi ratio of 1:1.[7] Because testing was performed in a particulate PEC system there was no way to apply a bias. Likewise a recent scanning electrochemical microscopy (SECM) study found that a V:Bi ratio of 1:1 resulted in the highest photocurrent when using an applied potential of 0.2 V vs Ag/AgCl in 0.1 M Na_2SO_4 along with 10 mM Na_2SO_3 as a sacrificial electron donor.[59]

We conducted PEC measurements in a variety of electrolyte solutions to further characterize the $BiVO_4$ films synthesized by RBD. Figure 9a shows the initial LSV scans for three films with different V/Bi ratios and surface treatments in 0.5 M Na_2SO_4. The film synthesized with V/Bi = 1 showed lower cathodic current (light and dark) at the start of the scan and a shift to purely anodic photocurrent at potentials more positive than −0.55 V vs Ag/AgCl. The film synthesized with V/Bi = 2 had a higher cathodic current (light and dark) with large transient spikes (cathodic and anodic) at the start of the sweep. A small amount of dark current, but essentially no photocurrent, was observed between −0.40 and 0.45 V vs Ag/AgCl at which point anodic onset was observed (similar to the LSV in Figure 1). Therefore, films synthesized with a V:Bi ratio of 1:1 do show higher photocatalytic activity as long as the applied potential is less positive than 0.45 V vs Ag/AgCl, but they fail to achieve a high maximum photocurrent at more positive potentials. Figure 9a shows that the addition of Co to the surface of the V/Bi = 1 film improved the maximum photocurrent by more than a factor of 3. Cobalt complexes are known to be electrocatalysts for water oxidation.[52,60−62] Another chopped LSV is shown in the Supporting Information (Figure S1) for the film synthesized with V/Bi = 2 after illuminating the film for 3 h at a constant potential of 1.0 V vs Ag/AgCl. It shows a more negative anodic onset potential, no dark current between −0.40 and 0.45

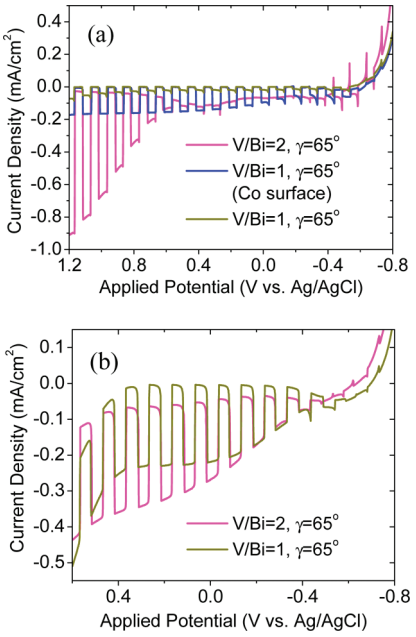

Figure 9. Chopped (dark and white light) LSV scans for films synthesized by RBD ($\gamma = 65°$, thickness = 0.5 μm) with different V/Bi ratios and surface treatments measured in (a) 0.5 M Na_2SO_4 and (b) 0.5 M Na_2SO_4 and 0.5 M Na_2SO_3. The scan rate was 0.025 V/s.

V vs Ag/Ag/Cl, and a lower maximum photocurrent at higher potentials. The small amount of dark current and lack of photocurrent initially observed for the V/Bi = 2 film was likely caused by excess vanadium (vanadium oxide) on the surface. Vanadium oxide dissolves readily in Na_2SO_4, and V_2O_5 electrodes have shown dark current for current vs potential scans in the range of −0.2 and 0.405 V vs SCE.[9,63]

Figure 9b shows LSV scans for two films in 0.5 M Na_2SO_4 and 0.5 M Na_2SO_3. The Na_2SO_3 was added to improve the surface kinetics of the oxidation reaction by providing a species (SO_3^{2-}) more easily oxidizable than water. In the combined electrolyte solution the V/Bi = 1 film had a maximum photocurrent that was much closer to that of the V/Bi = 2 film. This result provides evidence that pure $BiVO_4$ films were limited by the surface kinetics of the water oxidation reaction. Employing Na_2SO_3 also shifted the onset potentials to more negative values by increasing the pH of the solution, and it nearly eliminated the transient spikes for both films. Several researchers have characterized the anodic and cathodic transient spikes for Fe_2O_3 films, attributing the behavior to recombination or back reaction of photogenerated species (oxy or hydroxyl) on the surface.[63−65] For the $BiVO_4$ films synthesized by RBD, the transient spikes were primarily anodic but may still be caused by surface recombination or a back reaction at the surface, as they were nearly eliminated with the use of a redox species (SO_3^{2-}) which undergoes a facile, irreversible oxidation.

The chopped LSV scans in Figure 9a can be used to estimate the location of the flat band potential of the $BiVO_4$ films. For the V/Bi = 1 film, there was a clear transition from cathodic to anodic photocurrent around −0.55 V vs Ag/AgCl. The photocurrent transition was more difficult to distinguish for the V/Bi = 2 film because of the dark current. EIS measurements were performed on this film, and the resulting Mott−Schottky plot shown in Figure 10 indicates a flat band potential of approximately −0.7 V vs Ag/AgCl. After 3 h of PEC testing, the chopped LSV for the

dx.doi.org/10.1021/jp1109459 |J. Phys. Chem. C 2011, 115, 3794–3802

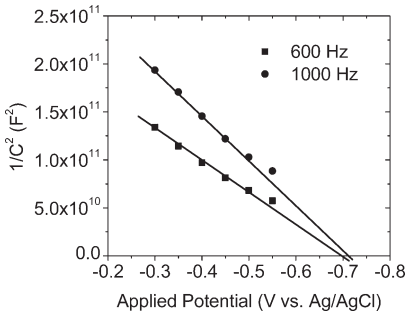

Figure 10. Mott−Schottky plot for $BiVO_4$ film synthesized by RBD (V/Bi = 2, γ = 65°, thickness = 0.5 μm). The measurement was conducted in 0.5 M Na_2SO_4.

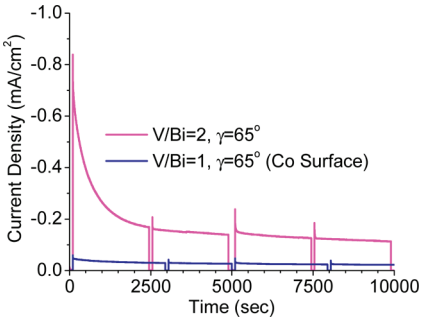

Figure 11. Amperometric $i-t$ curve for $BiVO_4$ films synthesized by RBD (γ = 65°, thickness = 0.5 μm) with different V/Bi ratios and surface treatments in 0.1 M Na_2SO_4 at a constant applied potential of 1.0 V vs Ag/AgCl.

V/Bi = 2 film shows a transition from cathodic to anodic current near −0.5 V vs Ag/AgCl (see Figure S1).

Film Stability and Surface Characterization. For any material to be practical in a large-scale energy conversion system, it must remain stable under illumination for long periods of time. There are limited reports in the literature on the long-term stability of $BiVO_4$. One group tested the stability of $BiVO_4$ synthesized by modified metal−organic decomposition and found that with a bias of 1.2 V applied to a Pt counter-electrode the photocurrent dropped from 2 mA/cm^2 to a steady-state value of 0.5 mA/cm^2 (~75% drop) in less than 1 h.[9] We conducted long-term PEC tests of $BiVO_4$ films in Na_2SO_4 solutions with a constant applied potential of 1.0 V vs Ag/AgCl as shown in Figure 11. The discontinuities in photocurrent were caused by blocking the white light source to confirm the photoactivity and stopping/restarting the potentiostat near 5000 s. The photocurrent of the film deposited with V/Bi = 2 film dropped by more than 70% before it reached a relatively steady-state value while the V/Bi = 1 film with Co on the surface reached a lower steady-state photocurrent almost immediately. Films deposited with V/Bi = 1 but without Co were also stable but had lower photoactivity as shown in Figure 9a.

A fraction of the photocurrent decay is caused by the build-up of oxygen bubbles on the film and local changes in pH. During PEC testing, oxygen bubbles formed and became trapped between the film surface and the O-ring on the glass electrochemical cell, reducing the geometric film surface area available for the reaction. In addition, the continuous oxidation of water produced H^+ ions, which decreased the pH of the electrolyte near the film, shifting the redox potentials and slowing down the reaction. This was verified by comparing the photocurrent in pure 0.5 M Na_2SO_4 and a mixture of 0.5 M Na_2SO_4 and 0.5 M phosphate buffer solution (pH 6.8). The steady-state photocurrent was about 20% higher in the buffer solution as compared to Na_2O_4 (see Figure S2 in Supporting Information).

Most of the photocurrent decay was caused by changes in the chemical composition of the film. We used XPS to measure the film surface before and after PEC testing. Initially the film deposited with an atomic flux ratio of V/Bi = 2 had a XPS measured V/Bi ratio of 1.54. The binding energies of the elements were found to be 159.0 eV for Bi 4f 7/2, 516.8 eV for V 2p 3/2, and 529.8 eV for O 1s, suggesting oxidation states of Bi^{3+}, V^{5+}, and O^{2-}.[66] After long-term PEC testing, the locations of these peaks remained the same but the intensities had changed and the XPS measured V/Bi ratio dropped to 0.51, indicating a loss of vanadium at the surface. Table 1 summarizes photocurrent and XPS results for PEC testing, and the XPS spectra are included in the Supporting Information (Figure S3). We could not use XPS to measure the concentration and oxidation states of elements below the surface. The argon sputter etch gun on the Kratos AXIS Ultra DLD spectrometer was mounted with an incident angle of 45°, and the $BiVO_4$ films had a porous structure so much of the film surface was shadowed during sputter etching. It is possible that the concentration of vanadium was higher in the bulk material than on the film surface.

To further characterize the decay in photocurrent, we used ICP-MS to measure Bi and V ion concentrations in the electrolyte before and after PEC testing. For the film deposited with V/Bi = 2, the V concentration in the electrolyte went from below the detection limits to 247 ppb after long-term PEC testing while the Bi concentration remained below detection. It is apparent that much of the initial photocurrent was due to photocorrosion of excess vanadium into the electrolyte. For the film with V/Bi = 1 and Co on the surface, the Bi and V concentrations in the electrolyte remained below the detection limits after long-term PEC testing. The ICP-MS results are tabulated in the Supporting Information (Table S1). Even though films synthesized with V/Bi = 2 show a loss of vanadium so that the atomic ratio is reduced, the steady-state photocurrent of these films is higher than the photocurrent of films that are initially synthesized with V/Bi = 1.

The film deposited with V/Bi = 1 may be limited by other factors in addition to slow surface kinetics. As shown in Figure 4, the film with V/Bi = 1 had a more gradual absorption line that became saturated near 460 nm, possibly due to scattering or reflection. This makes it difficult to accurately calculate the APCE and distinguish whether poor charge transport or slow surface kinetics is the greater limiting factor.

We attempted to stabilize the photocurrent of the films deposited with V/Bi = 2 by adding Ag or Co to the surface. Others have reported that pure $BiVO_4$ synthesized by metal−organic decomposition showed a decrease in photocurrent accompanied by a reduction of the V/Bi ratio at the surface when using a bias of 1.2 V applied to a Pt counter-electrode. When the surface was treated with $AgNO_3$, the initial photocurrent was higher and both the photocurrent and surface concentration remained fairly stable.[9] We treated films synthesized by RBD with $AgNO_3$ but did not see an increase in photocurrent or stability during three-electrode PEC measurements. Moreover, films treated with $AgNO_3$ showed a significant dark current during LSV scans moving more positive of 0.25 V vs Ag/AgCl. This was likely due to the oxidation of Ag. The addition of Co to the surface of films deposited with V/Bi = 2

dx.doi.org/10.1021/jp1109459 |J. Phys. Chem. C 2011, 115, 3794–3802

Table 1. Photocurrent and XPS Data for Film Synthesized by RBD (V/Bi = 2, $\gamma = 65°$, thickness = 0.5 μm) Taken before and after 3 h of Illumination in 0.5 M Na_2SO_4 at 1.0 V vs Ag/AgCl[a]

		atomic % (neglecting C)			
film condition	LSV photocurrent: +1 V vs Ag/AgCl	O 1s	V 2p	Bi 4f	V/Bi ratio
initial	0.91 mA/cm^2	66	21	14	1.54
after 3 h	0.36 mA/cm^2	71	10	20	0.51

[a] The concentration of Bi, V, O, and C were calculated from the integrated peak areas obtained after subtracting the background from each peak using the Shirley method.[51].

reduced the initial photocurrent by slowing down the photocorrosion of excess vanadium, but the final steady-state photocurrent was similar to that of films without Co on the surface. As shown in Figures 3b and 9a, Co treatment significantly enhanced the photocurrent and IPCE of films deposited with V/Bi = 1.

CONCLUSIONS

We have synthesized $BiVO_4$ films by reactive ballistic deposition (RBD) and reported on the photocatalytic activity for water oxidation. The photoactivity was higher for films deposited at more glancing angles of incidence ($\gamma = 45-75°$) than for films deposited at normal incidence ($\gamma = 0°$) primarily because of differences in surface structure and morphology. RBD was used to incorporate excess vanadium into $BiVO_4$ films, which increased the initial photocurrent at high applied potentials (1.0 V vs Ag/AgCl); however, the excess vanadium dissolved into the solution with time under illumination and a large portion of the initial photoactivity can be attributed to photocorrosion. The photocurrent dropped to a steady-state value that is still 1 order of magnitude greater than that for films synthesized with equal amounts of bismuth and vanadium, which were stable but limited by slow surface kinetics for the water oxidation reaction. The addition of Co to the surface of $BiVO_4$ films with equal bismuth and vanadium increases the photocurrent, but more work is needed to improve the light absorption and charge transport of these films so that they are closer to the maximum theoretical efficiency of a 2.3−2.4 eV bandgap material under AM1.5 illumination.

ASSOCIATED CONTENT

Supporting Information. An amperometric $i-t$ curve in phosphate buffer solution, XPS spectra, and ICP-MS data. This material is available free of charge via the Internet at http://pubs.acs.org.

AUTHOR INFORMATION

Corresponding Author
*mullins@che.utexas.edu.

ACKNOWLEDGMENT

C. B. Mullins and A. J. Bard acknowledge the National Science Foundation (CHE-0934450) and the Welch Foundation (F-1436 (C.B.M.) and F-0021 (A.J.B.)) for their generous support. S. P. Berglund thanks the National Science Foundation Graduate Research Fellowship Program for financial support and the University of Texas at Austin Cockrell School of Engineering for the Thrust 2000 Graduate Fellowship in Engineering (Harry P. Whitworth endowed). This work has also been partially supported by the U.S. Army Research Laboratory and U.S. Army Research Office (for C.B. M. under contract/grant number W911NF-09-0130). Finally, we acknowledge the Center for Electrochemistry at University of Texas at Austin supported by the Welch Foundation (grant H-F-0037). The National Science Foundation (Grant No. 0618242) funded the Kratos AXIS Ultra DLD spectrometer used for this study.

REFERENCES

(1) Fujishima, A.; Honda, K. *Nature* **1972**, *238*, 37.
(2) Kudo, A.; Miseki, Y. *Chem. Soc. Rev.* **2009**, *38*, 253.
(3) Osterloh, F. E. *Chem. Mater.* **2008**, *20*, 35.
(4) Bak, T.; Nowotny, J.; Rekas, M.; Sorrell, C. C. *Int. J. Hydrogen Energy* **2002**, *27*, 991.
(5) Maeda, K.; Domen, K. *J. Phys. Chem. C* **2007**, *111*, 7851.
(6) Bard, A. J.; Fox, M. A. *Acc. Chem. Res.* **1995**, *28*, 141.
(7) Kudo, A.; Omori, K.; Kato, H. *J. Am. Chem. Soc.* **1999**, *121*, 11459.
(8) Tokunaga, S.; Kato, H.; Kudo, A. *Chem. Mater.* **2001**, *13*, 4624.
(9) Sayama, K.; Nomura, A.; Arai, T.; Sugita, T.; Abe, R.; Yanagida, M.; Oi, T.; Iwasaki, Y.; Abe, Y.; Sugihara, H. *J. Phys. Chem. B* **2006**, *110*, 11352.
(10) Liu, H.; Nakamura, R.; Nakato, Y. *J. Electrochem. Soc.* **2005**, *152*, G856.
(11) Long, M.; Cai, W.; Cai, J.; Zhou, B.; Chai, X.; Wu, Y. *J. Phys. Chem. B* **2006**, *110*, 20211.
(12) Walsh, A.; Yan, Y.; Huda, M. N.; Al-Jassim, M. M.; Wei, S.-H. *Chem. Mater.* **2009**, *21*, 547.
(13) Oshikiri, M.; Boero, M.; Ye, J. H.; Zou, Z. G.; Kido, G. *J. Chem. Phys.* **2002**, *117*, 7313.
(14) Kohtani, S.; Yoshida, K.; Maekawa, T.; Iwase, A.; Kudo, A.; Miyabe, H.; Nakagaki, R. *Phys. Chem. Chem. Phys.* **2008**, *10*, 2986.
(15) Kudo, A.; Ueda, K.; Kato, H.; Mikami, I. *Catal. Lett.* **1998**, *53*, 229.
(16) Bard, A. J.; Faulkner, L. R. *Electrochemical Methods: Fundamentals and Applications*, 2nd ed.; John Wiley & Sons, Inc.: Hoboken, NJ, 2001.
(17) Yu, J.; Kudo, A. *Chem. Lett.* **2005**, *34*, 850.
(18) Xi, G. C.; Ye, J. H. *Chem. Commun.* **2010**, *46*, 1893.
(19) Galembeck, A.; Alves, O. L. *Thin Solid Films* **2000**, *365*, 90.
(20) Sayama, K.; Nomura, A.; Zou, Z.; Abe, R.; Abe, Y.; Arakawa, H. *Chem. Commun.* **2003**, 2908.
(21) Neves, M. C.; Trindade, T. *Thin Solid Films* **2002**, *406*, 93.
(22) Liu, J.; Wang, H.; Wang, S.; Yan, H. *Mater. Sci. Eng. B* **2003**, *104*, 36.
(23) Gotic, M.; Music, S.; Ivanda, M.; Soufek, M.; Popovic, S. *J. Mol. Struct.* **2005**, *744−747*, 535.
(24) Jiang, H.-q.; Endo, H.; Natori, H.; Nagai, M.; Kobayashi, K. *J. Eur. Ceram. Soc.* **2008**, *28*, 2955.
(25) Strobel, R.; Metz, H. J.; Pratsinis, S. E. *Chem. Mater.* **2008**, *20*, 6346.
(26) Dunkle, S. S.; Helmich, R. J.; Suslick, K. S. *J. Phys. Chem. C* **2009**, *113*, 11980.
(27) Ke, D.; Peng, T.; Ma, L.; Cai, P.; Jiang, P. *Appl. Catal. A* **2008**, *350*, 111.
(28) Yu, J.; Zhang, Y.; Kudo, A. *J. Solid State Chem.* **2009**, *182*, 223.

(29) Dall'Antonia, L. H.; de Tacconi, N. R.; Chanmanee, W.; Timmaji, H.; Myung, N.; Rajeshwar, K. *Electrochem. Solid-State Lett.* **2010**, *13*, D29.
(30) Castillo, N. C.; Heel, A.; Graule, T.; Pulgarin, C. *Appl. Catal. B* **2010**, *95*, 335.
(31) Rullens, F.; Laschewsky, A.; Devillers, M. *Chem. Mater.* **2006**, *18*, 771.
(32) Zhang, L.; Chen, D.; Jiao, X. *J. Phys. Chem. B* **2006**, *110*, 2668.
(33) Zheng, Y.; Wu, J.; Duan, F.; Xie, Y. *Chem. Lett.* **2007**, *36*, 520.
(34) Li, G.; Zhang, D.; Yu, J. C. *Chem. Mater.* **2008**, *20*, 3983.
(35) Zhou, L.; Wang, W.; Liu, S.; Zhang, L.; Xu, H.; Zhu, W. *J. Mol. Catal A: Chem.* **2006**, *252*, 120.
(36) Zhou, L.; Wang, W.; Zhang, L.; Xu, H.; Zhu, W. *J. Phys. Chem. C* **2007**, *111*, 13659.
(37) Su, J.; Guo, L.; Yoriya, S.; Grimes, C. A. *Cryst. Growth Des.* **2009**, *10*, 856.
(38) Zhang, H.; Liu, J.; Wang, H.; Zhang, W.; Yan, H. *J. Nanopart. Res.* **2008**, *10*, 767.
(39) Dohnálek, Z.; Kimmel, G. A.; McCready, D. E.; Young, J. S.; Dohnálková, A.; Smith, R. S.; Kay, B. D. *J. Phys. Chem. B* **2002**, *106*, 3526.
(40) Flaherty, D. W.; Dohnálek, Z.; Dohnálková, A.; Arey, B. W.; McCready, D. E.; Ponnusamy, N.; Mullins, C. B.; Kay, B. D. *J. Phys. Chem. C* **2007**, *111*, 4765.
(41) Flaherty, D. W.; Hahn, N. T.; Ferrer, D.; Engstrom, T. R.; Tanaka, P. L.; Mullins, C. B. *J. Phys. Chem. C* **2009**, *113*, 12742.
(42) Flaherty, D. W.; May, R. A.; Berglund, S. P.; Stevenson, K. J.; Mullins, C. B. *Chem. Mater.* **2009**, *22*, 319.
(43) Hahn, N. T.; Ye, H.; Flaherty, D. W.; Bard, A. J.; Mullins, C. B. *ACS Nano* **2010**, *4*, 1977.
(44) Hahn, N. T.; Mullins, C. B. *Chem. Mater.* **2010**, *22*, 6474.
(45) May, R. A.; Flaherty, D. W.; Mullins, C. B.; Stevenson, K. J. *J. Phys. Chem. Lett.* **2010**, *1*, 1264.
(46) Chen, Z. B.; Jaramillo, T. F.; Deutsch, T. G.; Kleiman-Shwarsctein, A.; Forman, A. J.; Gaillard, N.; Garland, R.; Takanabe, K.; Heske, C.; Sunkara, M.; McFarland, E. W.; Domen, K.; Miller, E. L.; Turner, J. A.; Dinh, H. N. *J. Mater. Res.* **2010**, *25*, 3.
(47) Li, M.; Zhao, L.; Guo, L. *Int. J. Hydrogen Energy* **2010**, *35*, 7127.
(48) Murakami, Y.; Ikarashi, M.; Hashizume, M.; Nosaka, A. Y.; Nosaka, Y. *Electrochem. Solid-State Lett.* **2008**, *11*, H42.
(49) Long, M.; Cai, W.; Kisch, H. *J. Phys. Chem. C* **2007**, *112*, 548.
(50) Chatchai, P.; Murakami, Y.; Kishioka, S.-y.; Nosaka, A. Y.; Nosaka, Y. *Electrochim. Acta* **2009**, *54*, 1147.
(51) Shirley, D. A. *Phys. Rev. B* **1972**, *5*, 4709.
(52) Kay, A.; Cesar, I.; Gratzel, M. *J. Am. Chem. Soc.* **2006**, *128*, 15714.
(53) Abelmann, L.; Lodder, C. *Thin Solid Films* **1997**, *305*, 1.
(54) Hawkeye, M. M.; Brett, M. J. *J. Vacuum Sci. Technol. A* **2007**, *25*, 1317.
(55) Movchan, B. A.; Demchish, A. V. *Phys. Metals Metallogr.-USSR* **1969**, *28*, 83.
(56) Higo, M.; Fujita, K.; Tanaka, Y.; Mitsushio, M.; Yoshidome, T. *Appl. Surf. Sci.* **2006**, *252*, 5083.
(57) Wagner, R. S.; Ellis, W. C. *Appl. Phys. Lett.* **1964**, *4*, 89.
(58) Smith, J. F. *J. Alloy Phase Diagrams* **1990**, *6*, 19.
(59) Ye, H.; Lee, J.; Jang, J. S.; Bard, A. J. *J. Phys. Chem. C* **2010**, *114*, 13322.
(60) Brunschwig, B. S.; Chou, M. H.; Creutz, C.; Ghosh, P.; Sutin, N. *J. Am. Chem. Soc.* **1983**, *105*, 4832.
(61) Svegl, F.; Orel, B.; Grabec-Svegl, I.; Kaucic, V. *Electrochim. Acta* **2000**, *45*, 4359.
(62) Kanan, M. W.; Nocera, D. G. *Science* **2008**, *321*, 1072.
(63) Hardee, K. L.; Bard, A. J. *J. Electrochem. Soc.* **1977**, *124*, 215.
(64) Iwanski, P.; Curran, J. S.; Gissler, W.; Memming, R. *J. Electrochem. Soc.* **1981**, *128*, 2128.
(65) Anderman, M.; Kennedy, J. H. *J. Electrochem. Soc.* **1984**, *131*, 21.
(66) Wagner, C. D.; Naumkin, A. V.; Kraut-Vass, A.; Allison, J. W.; Powell, C. J.; Rumble, J. R., Jr. *NIST X-ray Photoelectron Spectroscopy Database*, Gaithersburg, MD. http://srdata.nist.gov/xps/Default.aspx.